Human Molecular Genetics, 2012, Vol. 21, No. 22 **4876–4887**
doi:10.1093/hmg/dds324
Advance Access published on August 7, 2012

Impaired proteolysis underlies autophagic dysfunction in Niemann–Pick type C disease

Matthew J. Elrick[1,2,3], Ting Yu[1], Chan Chung[1] and Andrew P. Lieberman[1,*]

[1]Department of Pathology, [2]The Neuroscience Graduate Program and [3]The Medical Scientist Training Program, University of Michigan, Ann Arbor, MI 48109, USA

Received May 28, 2012; Revised July 20, 2012; Accepted August 2, 2012

Niemann–Pick type C disease (NPC) is a childhood onset neurodegenerative disorder arising from lipid-trafficking defects caused by mutations in the *NPC1* or *NPC2* gene. Marked accumulation of autophagosomes is a prominent feature of NPC cells, yet a detailed understanding of the disease-associated alterations in autophagy and their role in pathogenesis has been lacking. Prior studies have shown that lipid storage in NPC disease induces autophagy. Here, we additionally show that the clearance of autophagosomes in NPC1 deficiency is impaired due to inhibition of lysosomal protease activity by stored lipids. We also demonstrate that the autophagic pathway is a source of stored cholesterol in the NPC lysosome, thus creating a positive feedback loop wherein autophagy induction exacerbates the disease via increased lipid storage. Inhibition of autophagy reduces cholesterol storage and restores normal lysosomal proteolysis in NPC1-deficient cells, supporting a model in which activation of the autophagic pathway promotes disease pathogenesis.

INTRODUCTION

Macroautophagy (hereafter referred to as "autophagy") is the sequestration of cytoplasmic constituents into double-membrane bound organelles known as autophagosomes, and their subsequent delivery to lysosomes for degradation and recycling (1). Basal autophagy plays an important role in the turnover of proteins and organelles. Autophagy may also be induced in response to cellular stressors, such as nutrient depletion, endoplasmic reticulum stress and proteostasis defects. Recent progress has revealed a significant role for autophagy in health and disease, including cancer, immunity and neurodegeneration (2). Basal autophagy is an absolute requirement for neuronal homeostasis, as autophagy-deficient mouse mutants display neurodegeneration associated with the accumulation of ubiquitinated protein aggregates and the appearance of motor impairments (3,4). The promotion of autophagy has proven to be a beneficial therapeutic strategy in models of neurodegenerative protein aggregation disorders, presumably by facilitating turnover of the offending, misfolded protein (5). Conversely, excessive autophagy has also been implicated in neurodegeneration (6), although these findings remain controversial (7). In accordance with its putative roles in neurodegeneration, alterations of the autophagic pathway have been reported in multiple disorders, including Alzheimer, Parkinson and Huntington diseases, as well as many of the lysosomal storage diseases (8,9). In most cases, the relevance of these autophagic alterations to disease pathogenesis remains poorly defined and this represents a significant barrier to the use of autophagy as a therapeutic target.

Niemann–Pick type C disease (NPC) is one of ~50 lysosomal diseases, which collectively represent the most common cause of childhood neurodegeneration (10). NPC disease is characterized by ataxia, cognitive decline, seizures, dystonia, cataplexy and vertical supranuclear gaze palsy (11). It is caused by mutations in the *NPC1* or *NPC2* genes (12,13), whose protein products are thought to act cooperatively in the efflux of cholesterol from late endosomes and lysosomes (14). In NPC disease, unesterified cholesterol accumulates in late endosomes and lysosomes of all tissues, and is classically considered to be derived from receptor-mediated endocytosis of low density lipoprotein (LDL)-cholesterol (15). A broad array of glycosphingolipids accumulates as well (16), although it is unknown whether this latter phenomenon is attributable to a direct role for NPC1/NPC2 in glycosphingolipid trafficking or is secondary to cholesterol accumulation.

The storage of lipids in NPC disease has a number of cell biological consequences. One of the most striking among these is the marked accumulation of autophagic vesicles,

*To whom correspondence should be addressed at: Department of Pathology, University of Michigan Medical School, 3510 MSRB1, 1150 W. Medical Center Dr., Ann Arbor, MI 48109-0605, USA. Tel: +1 7346474624; Fax: +1 7346153441; Email: liebermn@umich.edu

which has been demonstrated in multiple tissues of *Npc1*$^{-/-}$ mice and cultured cells from human NPC patients (17,18). We have previously demonstrated that this elevated load of autophagic vesicles is associated with increased autophagic flux, and that this induction of autophagy is dependent upon Beclin-1 (18). However, the process of autophagy consists of multiple independently regulated components, and it is unknown whether NPC1 deficiency has separate effects on its induction and completion. Induction of autophagy is a multistep process that includes stimulation of the LC3 conjugation cascade, the formation of an isolation membrane and envelopment of cytoplasmic cargoes to form an autophagosome. Completion of autophagy requires microtubule-based trafficking of the autophagosome into the proximity of a lysosome, autophagosome-to-lysosome fusion to form an autolysosome, cargo degradation, efflux of degradation products and finally regeneration of the lysosome. The sum total of these steps is known as autophagic flux (19). Previous experiments have indicated that the flux of protein substrates through the autophagic pathway in NPC1-deficient cells is increased by ~25% (18). However, autophagosome numbers in these cells are many times higher than those from healthy controls (18). An accumulation of autophagosomes to this magnitude in the context of only a modest increase in autophagic flux suggests that there is a defect in the completion of autophagy. Impaired completion of autophagy in NPC disease is additionally supported by the accretion of autophagic substrates in the brains of *Npc1*$^{-/-}$ mice, including ubiquitinated proteins (20) and p62 (21). A recent report also demonstrated accumulation of mitochondrial fragments attributable to impaired autophagic clearance in the stem cell-derived neuronal model of NPC disease (22).

In the present study, we advance our understanding of the role of autophagy in NPC disease. Utilizing measurements of autophagic cargo handling and lysosomal activity in living cells, we demonstrate decreased lysosomal cathepsin activity, likely resulting from stored lipids, leading to impaired turnover of autolysosomes. Further, we show that autophagy is a source of stored cholesterol in NPC lysosomes, revealing a positive feedback loop between lipid storage and autophagy induction. Breaking this feedback loop, by way of autophagy inhibition, reduced lipid storage and restored lysosomal protease activity. These data demonstrate a deleterious role for autophagy in NPC disease pathogenesis, and suggest novel therapeutic approaches to lysosomal disorders.

RESULTS

Autolysosomal cargo degradation is impaired in NPC1-deficient cells due to decreased cathepsin activity

The available data suggest that NPC1 deficiency leads to both an induction of autophagy and an impairment in the clearance of autophagosomes. We previously demonstrated that autophagy induction in NPC1 deficiency is a Beclin-1-dependent process that is associated with increased autophagic flux (18). However, little is known about the mechanism underlying the proposed defect in autophagosome clearance. Inefficient turnover of autophagosomes might arise from disruption of autophagosome trafficking, autophagosome-to-lysosome fusion or degradation of cargo following fusion. To distinguish between these possibilities, we used a tandem-tagged LC3, consisting of LC3 fused to both GFP and mCherry (23). In acidic environments, GFP ceases to fluoresce while mCherry remains fluorescent, enabling the discrimination between relatively neutral autophagosomes (both green and red) and acidic autolysosomes (red only) (23). This tool allowed us to determine whether the impairment in autophagy completion occurs before or after the formation of autolysosomes. For example, if NPC1-deficient cells were incapable of properly trafficking autophagosomes or coordinating their fusion to lysosomes, one would expect a build-up of autophagosomes and a paucity of autolysosomes. Instead, NPC1-deficient cells displayed a similar proportion of autolysosomes as cells from healthy controls (Fig. 1). Furthermore, when autophagy was induced using rapamycin, thereby challenging cells with an increased autophagic load, NPC1 mutant cells displayed a marked increase in the proportion of autolysosomes. In contrast, control cells were capable of handling this challenge without accumulating excess autolysosomes (Fig. 1). Our results demonstrated that autophagosome-to-lysosome fusion was largely intact in NPC1 deficiency. However, because autolysosomes accumulated following induction of autophagy, these data suggested a reduced capacity for autolysosome clearance.

To directly test this notion, we utilized time lapse imaging of cells transfected with mCherry-GFP-LC3. To account for vertical movement of vesicles, we imaged cells in four planes of focus spanning the full thickness of the cell. These images were deconvolved and then projected into a single two-dimensional image for each time point. We tracked autophagosomes until they lost their green fluorescence, indicating a lysosomal fusion event. Following this event, we measured elapsed time until the red fluorescence disappeared, indicating degradation of LC3 within the autolysosome. mCherry-LC3 degradation therefore served as a marker for autolysosomal cargo degradation. The apparent shape and intensity of vesicles were often influenced by their movement between z-planes or their simultaneous capture in multiple z-planes. These features were therefore not analyzed, and vesicles were regarded only as present or absent for the purpose of this analysis. Using this system, control autolysosomes had a mean lifetime of 1.2 ± 0.2 min. In contrast, autolysosomes in NPC1-deficient cells had a markedly increased mean lifetime of 3.6 ± 0.8 min (Fig. 2A and B), thus confirming that LC3 degradation in autolysosomes from mutant cells was impaired. Interestingly, the distribution of autolysosome lifetimes in NPC1 mutant cells was much broader than that of wild-type cells, including many that were in the normal range, but others that persisted for as long as 18 min (Fig. 2C).

To further confirm this finding, we sought to use a non-LC3-dependent readout for lysosome function. We hypothesized that impaired autolysosomal cargo degradation was due to reduced lysosomal cathepsin activity. To test this, we used Magic Red, a commercial reagent consisting of a fluorophore covalently bound to a di-arginine peptide motif that quenches the fluorophore and targets the molecule for cleavage by cathepsin B. Prior to cleavage, Magic Red is cell permeable and non-fluorescent. Following cleavage, it becomes trapped in lysosomes and fluoresces red. The rate

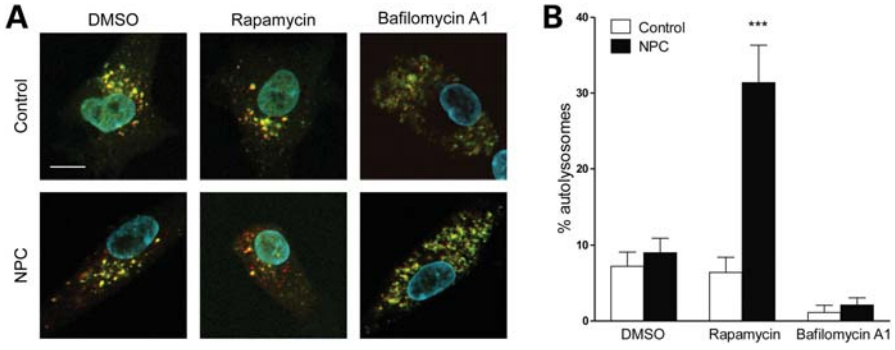

Figure 1. Intact autophagosome–lysosome fusion, but impaired autolysosome clearance in NPC1-deficient cells. (**A**) Representative images of human dermal fibroblasts transfected with mCherry-GFP-LC3, followed by 24 h treatment with vehicle (DMSO), 1 μM rapamycin, or 100 nM bafilomycin A1. Bafilomycin A1 treatment was included as a negative control, as it neutralizes the pH of lysosomes. Scale bar, 10 μm. (**B**) Quantification of the percent of total puncta that are autolysosomes (i.e. red only). $n = 8–10$ cells per group, pooled from two independent experiments. $^{***}P < 0.001$. Error bars are SEM.

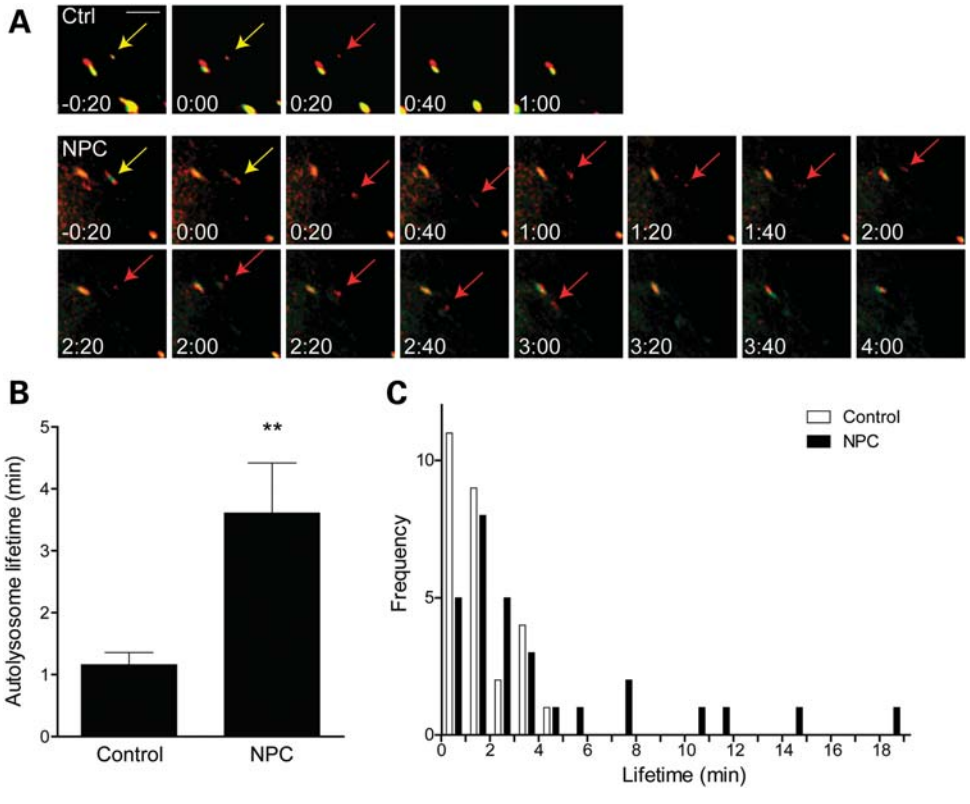

Figure 2. Prolonged lifespan of autolysosomes in NPC1-deficient cells. (**A**) Representative live cell time lapse images from human dermal fibroblasts demonstrating the fusion of an autophagosome (yellow) with a lysosome to form an autolysosome (red), followed by maturation of the autolysosome, as indicated by the loss of red signal. Note that autophagosomes move within the field during the experiment. Arrow indicates location and color of the autophagosome being measured. Scale bar, 2 μm. (**B**) Average lifetime of autolysosomes. $n = 27$ (Control) or 29 (NPC1) fusion events from four independent experiments. (**C**) Histogram of data presented in D. $^{**}P < 0.01$. Error bars are SEM.

of accumulation of red fluorescence in lysosomes was therefore used to estimate cathepsin activity *in situ*. To confirm the specificity of this reagent, we treated cells with bafilomycin A1 to disrupt lysosomal pH, and therefore enzyme activity, and found that this completely abolished the appearance of red fluorescence (Supplementary Material, Fig. S1). This assay revealed that cathepsin B activity in NPC1 null lysosomes was approximately half that of lysosomes in control cells (Fig. 3A–C). Similar analysis using an independent line of NPC1 null fibroblasts also demonstrated impaired cathepsin B activity (Supplementary Material, Fig. S2A). Furthermore, a distinct Magic Red reagent that is a specific substrate for cathepsin L demonstrated decreased activity, suggesting that functional impairment of cathepsin activity in mutant cells is a general feature of NPC1 deficiency (Supplementary Material, Fig. S2B).

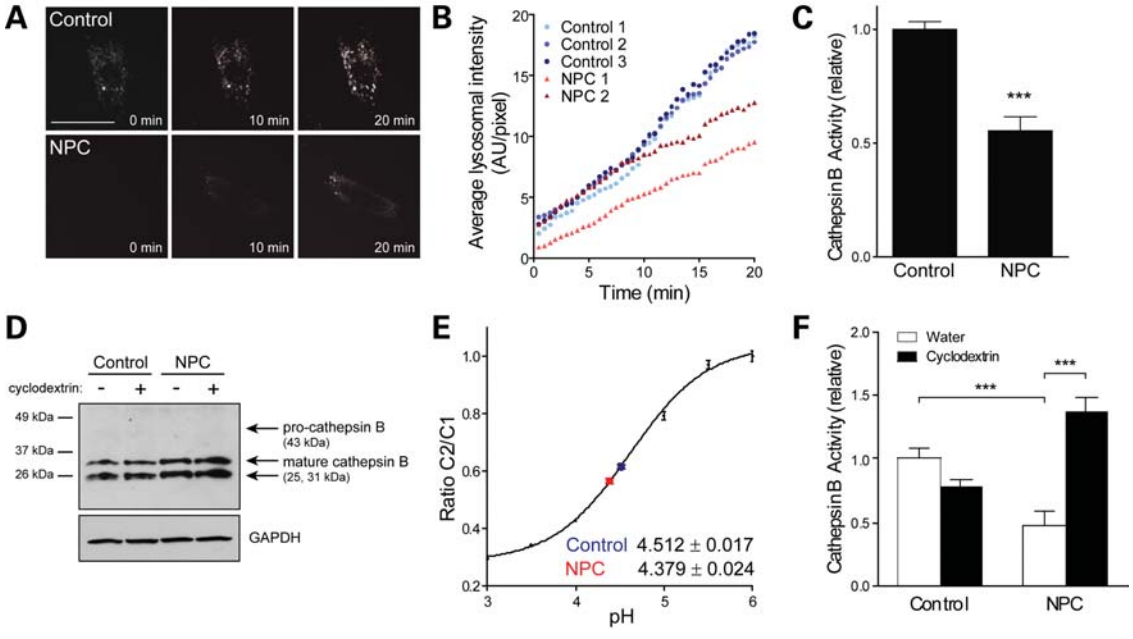

Figure 3. Lipid storage inhibits lysosomal proteolysis. (**A**) Representative time lapse images of human dermal fibroblasts treated with Magic Red Cathepsin B substrate. Scale bar, 50 μm. (**B**) Fluorescence intensity, normalized to total lysosomal area, from one representative experiment. (**C**) Relative cathepsin B activity, as determined by the slope of the fluorescence intensity plots. $n = 7–9$ fields of cells per group, from three independent experiments. (**D**) Western blot for cathepsin B in human dermal fibroblast lysates, following 24 h treatment with 300 μM cyclodextrin or vehicle (water). Procathepsin B was undetectable in both cell lines, except at very long exposures (data not shown). (**E**) Lysosomal pH, measured by ratiometric imaging following uptake of Oregon Green dextran. Standard curve is shown in black. Extrapolated data points are shown in blue (control) and red (NPC). $n = 34–92$ cells for points on standard curve, 181 cells for Control, 141 cells for NPC. (**F**) Relative cathepsin B activity measured following 24 h treatment with 300 μM cyclodextrin or vehicle. $n = 9$ fields of cells per group, from three independent experiments. $^{***}P < 0.001$. Error bars are SEM.

We next sought to determine the mechanism underlying reduced cathepsin B activity in NPC1 lysosomes. Proper cathepsin activity requires the trafficking of inactive procathepsins to late endosomes, where they are cleaved into lower molecular weight active forms. These cleaved cathepsins become proteolytically active upon arrival in the low-pH environment of the lysosome (24). Proper trafficking and cleavage of procathepsins can therefore be confirmed by demonstration of mature cathepsins by western blot. Normal quantities of mature cathepsin B were found in NPC1 lysates, indicating that decreased cathepsin B activity was not due to defects in its processing (Fig. 3D). Prior studies have linked diminished lysosomal proteolysis in some lipid storage disorders to increased lysosomal pH (25,26). To determine whether dysregulation of lysosomal pH could account for impaired proteolysis in NPC1 lysosomes, lysosomal pH was measured using Oregon Green Dextran (27). This dextran conjugate is taken up by bulk phase endocytosis, arriving eventually at the lysosome. Oregon Green has two excitation maxima, one which is pH-sensitive and one which is pH-insensitive, enabling ratiometric imaging to estimate the pH of the lysosome. This technique demonstrated that the pH of NPC1 lysosomes was not elevated (Fig. 3E).

Having ruled out the common causes of cathepsin inhibition, we reasoned that the lipids stored in NPC1 lysosomes may be directly responsible for this phenomenon. To test this hypothesis, we treated NPC1-deficient cells with cyclodextrin, a compound that circumvents NPC1/NPC2 to clear lipid storage from NPC lysosomes (28,29) (Supplementary Material, Fig. S3). This treatment not only rescued cathepsin activity, but lead to a rebound above wild-type levels, reflective of the slight overexpression of cathepsin B in these cells (Fig. 3F). Therefore, NPC1 itself is not necessary for cathepsin activity. We conclude that the most likely explanation for the observed impairment of lysosomal cathepsin activity and autophagic substrate degradation is a direct inhibition of lysosomal proteases by stored lipids.

Autophagy is a source of stored cholesterol in NPC disease

We next wondered whether there was an interaction between the elevated levels of autophagosome formation in NPC1 disease and the observed defects in lysosome function. Autophagic sequestration of membrane-bound organelles would be expected to deliver a variety of lipids to the lysosome. Further, autophagy is known to transport lipid droplets into the lysosome through a recently described process known as macrolipophagy (30). Lipid droplets are cholesterol- and triglyceride-containing organelles, in which cholesterol is present in its esterified form (31). Cholesterol esters delivered to lysosomes through autophagy undergo hydrolysis by lysosomal acid lipase, an enzyme that remains active in NPC1 deficiency (32). Macrolipophagy would therefore be expected to increase the storage of unesterified cholesterol in NPC1-deficient cells, and therefore exacerbate disease phenotypes. To initially test this notion, we reversed the baseline autophagy induction in NPC1-deficient cells using the phosphatidylinositol 3 kinase (PI3K) inhibitors wortmannin and LY294002, each of which is a potent inhibitor of autophagosome formation. Pharmacological inhibition of PI3K activity

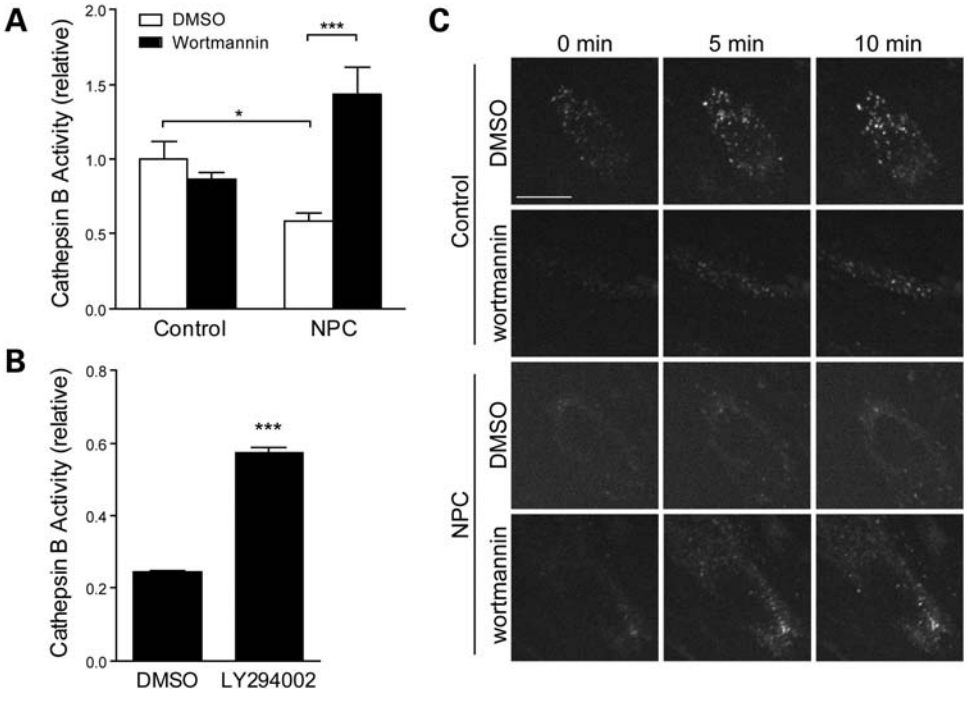

Figure 4. PI3 kinase inhibitors rescue cathepsin activity. (**A**) Relative cathepsin B activity following 72 h treatment with 250 nM wortmannin or DMSO. $n = 9$ fields of cells per group, from three independent experiments. (**B**) Relative cathepsin B activity following 72 h treatment of NPC1-deficient fibroblasts with 20 uM LY294002 or DMSO. $n = 3$ fields of cells per group. (**C**) Representative images from the experiment quantified in (A). Scale bar, 30 μm.$^{*}P < 0.05$, $^{***}P < 0.001$. Error bars are SEM.

with these two small molecules led to a rescue of cathepsin B activity in NPC1 mutant cells (Fig. 4) similar to that achieved by cyclodextrin.

These findings prompted us to directly test the extent to which autophagy modulates lipid storage in NPC1 cells. We first treated fibroblasts from NPC1 patients with rapamycin to further induce autophagy, and then quantified total lipid levels by high performance thin layer chromatography (HPTLC). Autophagy induction led to a significant increase in unesterified cholesterol in NPC fibroblasts, but not in normal controls (Fig. 5A). We also tested the effects of rapamycin on a panel of glycosphingolipids known to be stored in NPC1 fibroblasts. Of these, only glucosylceramide showed a modest increase following rapamycin treatment, while lactosylceramide and globotriaosylceramide were unaltered (Fig. 5B). Sphingomyelin levels were also measured, but this lipid was not stored in NPC1 cells under our culture conditions (Supplementary Material, Fig. S4). From these data, we concluded that autophagy does influence lipid storage in NPC1 cells. Cholesterol was the lipid most significantly affected by autophagy, and was therefore the focus of subsequent analyses.

For further experiments, we utilized filipin, a dye that stains unesterified cholesterol *in situ*, allowing the use of imaging techniques to assess cholesterol levels specifically in lipid storage organelles (LSO). Confirming the HPTLC results, rapamycin treatment modestly enhanced filipin staining of NPC1 fibroblasts, whereas treatment with the PI3K inhibitors wortmannin or LY294002 decreased filipin staining (Fig. 5C and D). Because the effects of PI3K inhibitors are not completely specific to autophagy, we next sought to confirm these results using genetic manipulation of autophagy. To achieve this, we used *Atg5* null MEFs, which are incapable of forming autophagosomes (33). To model NPC disease in these cells, they were treated with U18666A, a small molecule that induces a lipid storage phenotype identical to that of NPC disease (34). Following U18666A treatment, $Atg5^{-/-}$ MEFs developed considerably less filipin staining than wild-type MEFs (Fig. 5E). Together, these results indicate that autophagic delivery of endogenous lipids contributes to the cholesterol storage in NPC disease.

p62 accumulates in NPC neurons *in vivo*

To assess the function of the autophagic pathway *in vivo*, we stained brain tissue from $Npc1^{-/-}$ mice for p62/Sequestosome1, a multifunctional protein that seeds aggregates of ubiquitinated proteins and functions as an adapter for their recognition by the isolation membrane (23). As a substrate for the autophagic pathway, p62 levels are inversely correlated with autophagic flux (19). p62 staining was found in small punctuate structures throughout multiple brain regions of $Npc1^{-/-}$ mice (Fig. 6A). Strikingly, this staining pattern correlated tightly with the regions in which neuron death and severe pathology have been documented in NPC1 disease: cerebellum, prefrontal cortex, deep layers of the remainder of the cortex and multiple nuclei within the thalamus and brainstem (35–37).

We next asked which cell types were affected by p62 pathology. p62 puncta were present in cells with nuclei positive for the neuronal marker NeuN in the cortex and in calbindin-

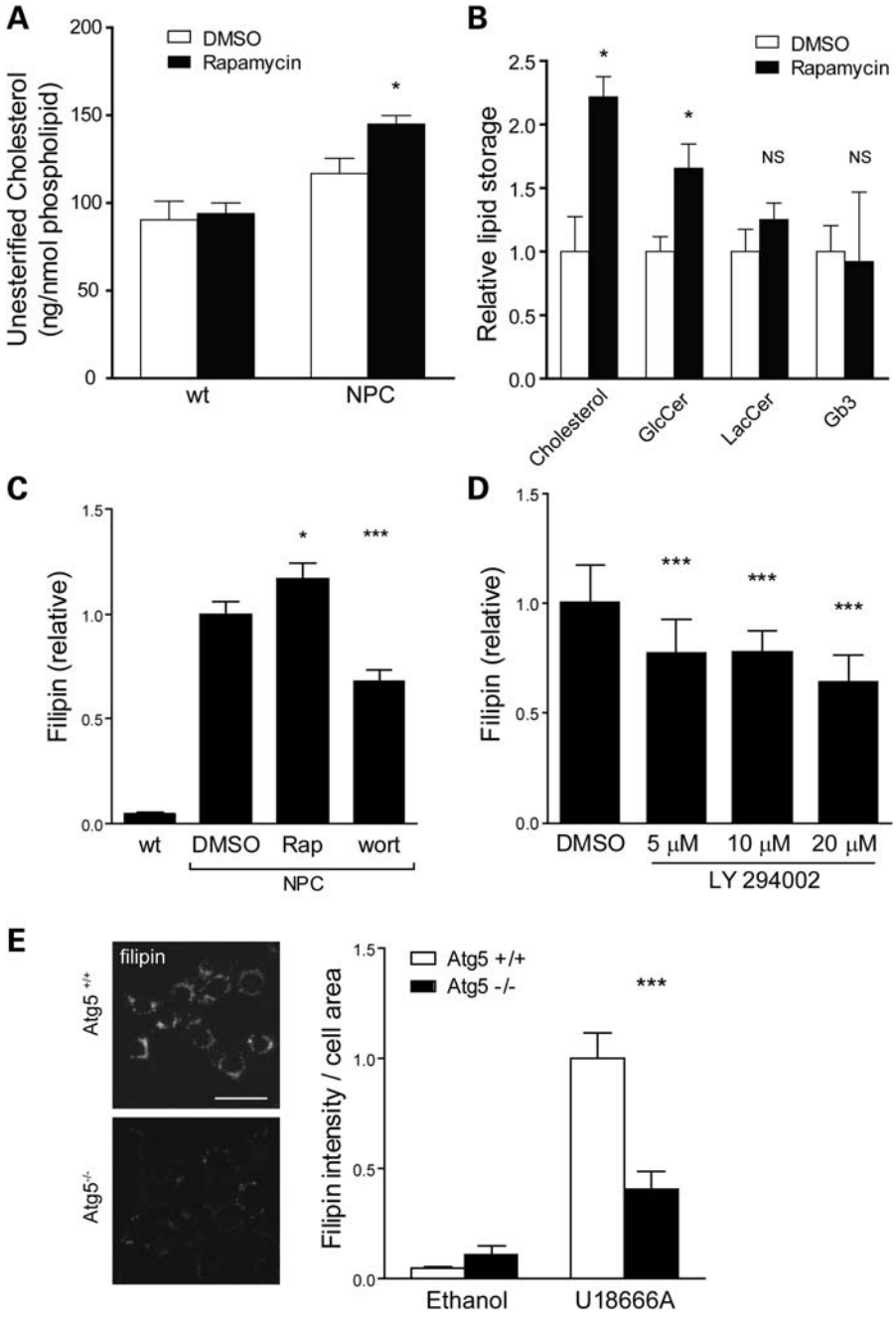

Figure 5. Autophagy contributes to lipid storage in NPC1-deficient cells. (**A**) Human dermal fibroblasts were treated with 1 μM rapamycin or vehicle (DMSO) for 24 h. Lipids were then extracted and total cellular unesterified cholesterol content was measured by HPTLC. $n = 8$ plates of cells per group, pooled across three independent experiments. (**B**) Summary of HPTLC data for total cellular content of cholesterol, glucosylceramide, lactosylceramide and globotriaosylceramide following treatment with 1 μM rapamycin or vehicle (DMSO) for 24 h. "Storage" is defined as the difference in absolute lipid content between NPC cells and DMSO-treated wild-type cells. For ease of comparison, data are normalized such that the relative storage of each lipid in DMSO-treated NPC cells equals one. GlcCer, galactosyl ceramide; LacCer, lactosyl ceramide; Gb3, globotriaosylceramide. (**C**) Human dermal fibroblasts were treated with DMSO, 1 μM rapamycin, or 250 nM wortmannin for 24 h. Stored cholesterol was stained with filipin, and the intensity of filipin staining was quantified by image analysis. $n = 15$ fields of cells, pooled across three independent experiments. (**D**) NPC1-deficient human dermal fibroblasts were treated with LY294002 at the indicated concentrations, or with vehicle (DMSO) for 72 h. Cholesterol storage was analyzed by filipin staining and image analysis. $n = 20$ fields of cells from two independent experiments. $^{*}P < 0.05$, $^{***}P < 0.001$. (**E**) Wild-type or Atg5$^{-/-}$ MEFs were treated with 1 μg/ml U18666A or vehicle (ethanol) for 24 h and then stained with filipin to demonstrate cholesterol storage. (Left panel) Representative images of filipin staining in U18666A-treated MEFs. Scale bar, 50 μm. (Right panel) Quantification of filipin intensity across three independent experiments, $n = 12–15$ fields of cells per group in total. Error bars are SEM.

positive Purkinje cells in the cerebellum (Fig. 6B). In contrast, p62 puncta were not identified in cells expressing the astrocyte marker GFAP or microglial marker Iba1 (Fig. 6B). Within neurons, p62 puncta partially colocalized with ubiquitin, but not with LC3 or Lamp1 (Fig. 6C). These data demonstrate that p62 did not accumulate within autophagosomes or

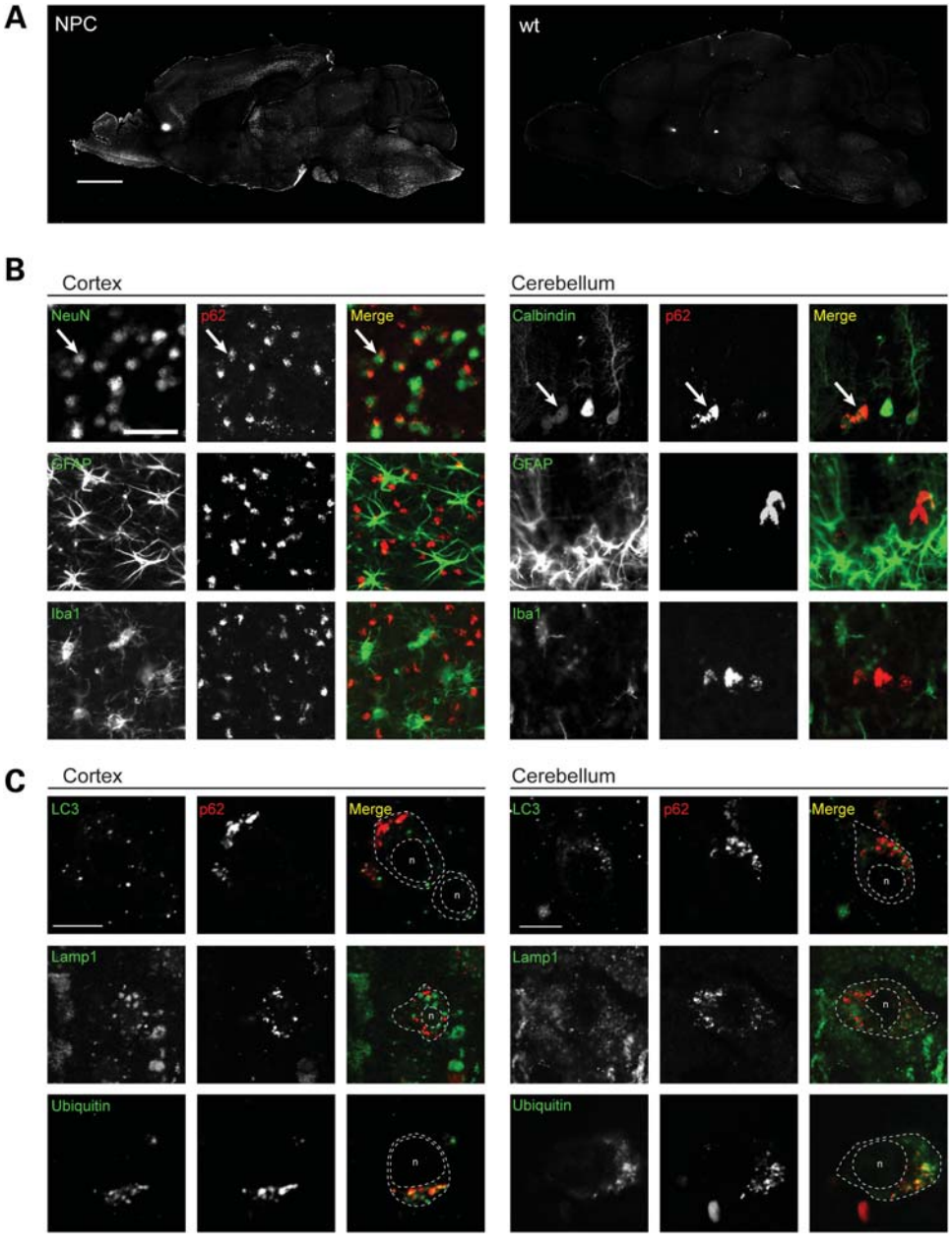

Figure 6. Autophagic substrate p62 accumulates in neurons *in vivo*. (**A**) Immunofluorescent staining for p62 in $Npc1^{-/-}$ or wild-type mouse brain. Scale bar, 2 mm. (**B**) Co-immunofluorescent staining for p62 (red) or markers (green) of neurons (NeuN, neuronal nuclei; or calbindin, Purkinje cells), astrocytes (GFAP) or microglia (Iba1) in $Npc1^{-/-}$ mice. Arrows indicate examples of a cell positive for both a neuronal marker and p62. Scale bar, 50 μm. (**C**) Confocal microscopy for colocalization of p62 (red) and autophagosomes (LC3), late endosomes and lysosomes (Lamp1) or ubiquitinated proteins (green). Dotted lines denote plasma membrane and nucleus (*n*). Scale bars, 10 μm.

lysosomes, but instead suggest its localization to cytoplasmic aggregates containing ubiquitinated proteins. These aggregates did not colocalize with typical aggresome markers such as proteasomal subunits or heat shock proteins, nor with signaling proteins that are known to interact with p62, including TRAF6, caspase-8 or ALFY (Supplementary Material, Fig. S5). These findings corroborate impaired clearance of autophagic substrates *in vivo*, and divulge a strong spatial correlation between autophagic dysfunction and cellular vulnerability to degeneration in NPC disease.

DISCUSSION

The data presented here help define the role of autophagy in NPC1 pathogenesis and provide novel insights into lysosomal dysfunction in NPC1 disease. We integrate these data into a model (Fig. 7) in which stored cholesterol arrives at the lysosome by both endocytic and autophagic routes. Here, it inhibits cathepsin activity, leading to the impaired turnover of autolysosomes and accumulation of autophagic intermediates. Previously reported data have also demonstrated that lipid storage causes

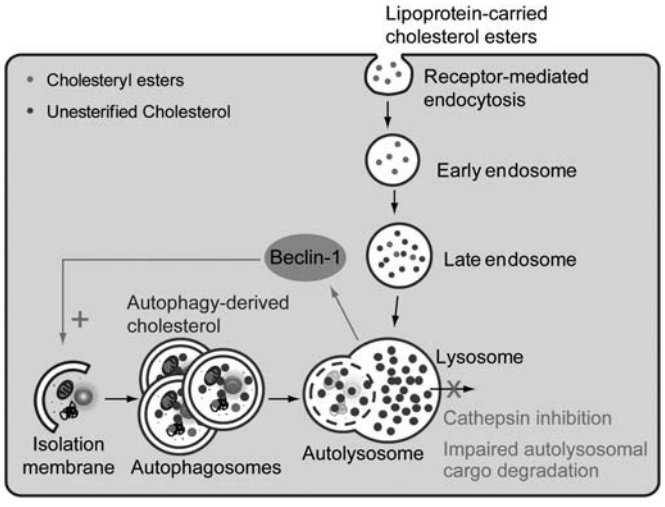

Figure 7. Model for the role of autophagy in NPC1 disease. Stored cholesterol arrives at the lysosome by two routes: receptor-mediated endocytosis of LDL-cholesterol and autophagic delivery of cholesterol. Lipid storage has two simultaneous effects on the autophagic pathway. First, it induces autophagy through a Beclin1-dependent (18). Second, it inhibits lysosomal cathepsins, leading to impaired degradation of lysosomal cargoes. The results of these events are increased rate of autophagosome generation, mildly increased autophagic flux and an accumulation of autophagic intermediates. Further, because autophagy delivers cholesterol to the lysosome, a positive feedback loop is created that promotes further lipid storage and lysosomal dysfunction.

autophagy induction (18,38). Autophagy induction enhances the delivery of cholesterol to the lysosome, thus creating a positive feedback loop that promotes NPC1 pathogenesis.

A key finding of our study is impaired degradation of autolysosomal cargoes. To demonstrate this, we developed a method for measuring the lifetime of individual autolysosomes. We were unable to find previous examples of such a measurement in the literature; however, estimates of the half-life of autophagosomes, encompassing all stages of the autophagic process, have been on the order of 10 min (39–41), consistent with our measurement of autolysosome turnover of ~1 min. That NPC1 autolysosomes showed marked variability in their rate of cargo degradation and took, on average, three times as long to degrade their cargoes, provided strong evidence of autolysosomal dysfunction in NPC disease. This variability might be accounted for by differing levels of lipid storage among autolysosomes. For example, autolysosomes formed via fusion with a nascent lysosome would be expected to contain less lipid than those resulting from fusion with a lysosome that has already accumulated a large lipid burden.

The observation of impaired autolysosome clearance led us to discover an underlying defect in lysosomal cathepsin activity, suggesting that the impairment of autolysosomal cargo degradation arises from a more general defect in lysosome function. Critical to this finding was the measurement of cathepsin activity *in situ* rather than in cell lysates, where overexpressed cathepsins removed from the context of the lipid-loaded lysosome have appeared to exhibit elevated activity (42). Our data support the notion that the inhibition of cathepsin activity in the NPC1 lysosome is due to the presence of cyclodextrin-sensitive lipid storage material rather than to alterations in cathepsin maturation or lysosomal pH, or to a direct requirement for NPC1 itself in proteolysis. Interestingly, a recent study demonstrated that loading cells with glycosphingolipids leads to similar alterations of the autophagic pathway as those reported here: autophagy induction, decreased clearance of autophagosomes and accumulation of autophagy intermediates (43). This raises the possibility that one or more glycosphingolipids, rather than cholesterol, may be responsible for alterations of the autophagic pathway in NPC disease. Therefore, the primary storage lipid and the pathogenic storage lipid(s) in this disorder may not be one and the same.

We did not find evidence of impaired autophagosome to lysosome fusion in NPC1-deficient cells. This mechanism is present in multiple sulfatase deficiency and mucopolysaccharidosis type IIIA (8). While our experiments may not have detected subtle defects in fusion, our data indicate that, if present, such a defect is not the major contributor to autophagic deficits in NPC1 disease. The absence of this phenomenon is unexpected in light of the existing literature on lysosomal fusion defects due to NPC1 deficiency. The fusion of late endosomes to lysosomes in NPC1 cells is markedly impaired, apparently due to the effects of cholesterol accumulation on Rab7-mediated anterograde vesicular trafficking (44,45). This phenomenon appears to extend to phagosomes as well (46). Rab7 is also involved in autophagy, and is required for autophagosome to lysosome fusion (47,48). Despite the expectation that cholesterol storage would also interfere with Rab7-mediated autophagosome maturation, we observed a normal ratio of autolysosomes to autophagosomes in NPC1 cells. Further, autophagy induction increased the cellular content of autolysosomes, providing further evidence that autophagosome to lysosome fusion is intact in these cells. It is not certain why lipid storage did not have the anticipated effect on autophagosome trafficking and fusion, but the answer may lie in the fact that the autophagic pathway relies on Rab7 effectors that are at least partially distinct from those involved in endocytosis (49). Given the above observations, impaired lysosomal proteolysis appears to be the primary barrier to the completion of autophagy in these cells. It should be considered that inhibition of lysosomal proteases may also contribute to the impairment of autophagy in other lysosomal diseases.

Previously, stored cholesterol in NPC lysosomes has been considered to be derived exclusively from the endocytic pathway via receptor-mediated endocytosis of LDL-cholesterol (15,50). However, we demonstrate here that deletion of the critical autophagy gene *Atg5* or treatment with autophagy inhibitors reduces cholesterol storage in NPC1 cellular models. This autophagic delivery of lipid likely reflects the sequestration of membrane-bound organelles plus delivery of cholesterol-containing lipid droplets through a recently described process known as macrolipophagy (30). By demonstrating involvement of autophagy in NPC1 lipid storage, we reveal a novel contribution of macrolipophagy to disease. Supporting this conclusion, inhibition of autophagy reduced cholesterol storage and rescued lysosomal dysfunction. The extent to which autophagy contributes to NPC pathology likely varies among cell types, depending on the relative balance between endocytosis and autophagy in a given cell.

The identification of decreased proteolytic activity in the NPC1 lysosome raises the possibility that all pathways delivering protein cargoes to the diseased lysosome could be impaired, leading to a broader proteostasis defect. Compounding this problem is the accumulation of p62, which has the ability to sequester ubiquitinated proteins that may otherwise have undergone proteasomal degradation (51). Alterations in the proteostasis network are a common feature of neurodegenerative diseases (52,53), and we speculate that similar defects occur in the NPC brain. Parallels between the neuropathology of NPC and several age-dependent protein aggregation neurodegenerative disorders have been noted, and include the accumulation of hyperphosphorylated tau, α-synuclein and beta-amyloid (54–58). Furthermore, it has been suggested that a prolonged half-life of autophagosomes may be detrimental through several mechanisms, including increased generation of beta-amyloid aggregates (59) and production of reactive oxygen species (60). We propose that impaired protein quality control due to lysosomal dysfunction underlies many of these changes in the NPC brain, and that proteostasis defects and the accumulation of autophagosomes and their cargoes contribute to the development of NPC neuropathology.

MATERIALS AND METHODS

Reagents

Hydroxy-β-propyl-cyclodextrin was from Cyclodextrin Technologies. Magic Red Cathepsin B substrate was from Immuno-Chemistry Technologies. Oregon Green Dextran was from Invitrogen. All other chemicals were from Sigma. Concentration and duration of drug treatments were as described in figure legends. The mCherry-GFP-LC3 plasmid was a gift from Terje Johansen (University of Tromsø). Antibodies used were: LC3 (Novus NB600-1384), GAPDH (Abcam ab8245), cathepsin B (Abcam ab33538), p62 (Novus H00008878-M01), NeuN (Millipore MAB-377), GFAP (Dako Z0334), Iba1 (Wako 019-19741), Lamp1 (Iowa Hybridoma Bank 1D4B) and ubiquitin (Dako Z0458).

Mice

npc1^{nih} Balb/cJ mice were obtained from Jackson Laboratories (#003092) and backcrossed to C57BL6/J for more than 10 generations. Genotyping was performed as previously described (61). *Npc1*$^{-/-}$ mice were generated as F1 hybrids between *Npc1*$^{+/-}$ mice on the C57BL6/J and Balb/cJ backgrounds, respectively. This method was found to restore Mendelian frequency of the *Npc1*$^{-/-}$ genotype, and therefore yielded experimental animals more efficiently than on either inbred background. All animal procedures were approved by the University of Michigan Committee on the Use and Care of Animals.

Cell culture and transfection

Human dermal fibroblast lines GM08399 (healthy control) and GM03123 (NPC disease; compound heterozygous for I1061T and P237S mutations in *NPC1*) were obtained from Coriell Cell Repositories, and were maintained in MEM (Gibco), supplemented with 15% FBS (Atlanta Biologicals), 10 μg/ml penicillin, 10 μg/ml streptomycin and 2 mM glutamine (Gibco). Atg5 MEF cell lines RCB2710 and RCB2711 were obtained from the RIKEN BRC Cell Bank, and were maintained in DMEM (Gibco) containing 10% FBS, 10 μg/ml penicillin, 10 μg/ml streptomycin and 2 mM glutamine. Plasmid transfection was performed by electroporation using a Nucleofector II (Lonza) per manufacturer's instructions.

Western blotting

Cells were lysed in RIPA buffer (Thermo Scientific) including c*O*mplete protease inhibitor tablets (Roche) and Halt phosphatase inhibitor (Thermo Scientific). Samples were electrophoresed through a homemade 10% SDS–PAGE gel. Samples were then transferred to nitrocellulose membranes (BioRad) using a semidry transfer apparatus. HRP-conjugated secondary antibodies were from BioRad. Blots were developed using TMA-6 (Lumigen) chemilluminescence reagent, following the manufacturer's protocols.

Lipid analysis

Lipids were isolated from cultured human skin fibroblasts and analyzed by HPTLC as previously described (62,63). Total phospholipid concentration was determined by lipid phosphate assay to ensure equal sample loading (64). Cholesterol was analyzed on HPTLC plates (EMD Chemicals) using a solvent system consisting of chloroform/glacial acetic acid (9:1). For analysis of glycosphingolipids, samples were subjected to further purification by alkaline methanolysis and acid hydrolysis (65). The samples were first resolved in chloroform/methanol (98:2), and then subjected to an additional resolution step in chloroforom/methanol/water/glacial acetic acid/concentrated ammonium hydroxide (64:31:3:2:0.5). HPTLC plates were developed by charring at 150°C following incubation with 8% $CuSO_4$ in methanol/water/H_3PO_4 (60:32:8). Lipid levels were quantified by densitometry using NIH ImageJ software, by extrapolation from a standard curve constructed from standards (cholesterol: Sigma, all others: Matreya) that were run on the same plate.

Filipin staining

Cells were grown on glass chamber slides (Lab-Tek) and stained with filipin as previously described (18). Images were captured on a Zeiss Axioplan 2 imaging system equipped with a Zeiss AxioCam HRc camera, with a 10× Zeiss EC Plan-NEOFLUAR objective, NA of 0.3, using AxioVision 4.8 software. Quantitative analysis of filipin images was performed using NIH ImageJ software, based on the "LSO compartment ratio assay" method (66). Images were thresholded to include only LSO, recognized as punctate filipin-stained structures. The integrated density of these thresholded images was measured. Then, a second lower threshold was set to include the fainter filipin staining of plasma membrane cholesterol, thereby defining the footprint of each cell in the field. The area of the thresholded region was measured to determine total cell area. Values reported are the integrated density of LSO filipin staining, divided by total cell area. These are

reported in arbitrary units, normalized such that the control group equals 1.

Histology

Mice were anesthetized with isofluorane and perfused transcardially with 0.9% normal saline followed by 4% paraformaldehyde. Brains were removed, bisected and post-fixed in 4% paraformaldehyde overnight. Brain tissue was cryoprotected in 30% sucrose for 48 h at 4°C, and then frozen in isopentane chilled by dry ice and embedded in OCT (Tissue-Tek). Staining was performed on free floating sections, prepared at 30 μm thickness. Widefield fluorescent images were captured on a Zeiss Axioplan 2 imaging system, as described above. Confocal microscopy was performed using a Zeiss LSM 510-META Laser Scanning Confocal Microscopy system, with a ×63 Zeiss C-Apochromat water immersion objective, NA of 1.2, using Zeiss LSM 510-META software.

Autophagosome fusion and degradation assays

Fibroblasts were transfected with mCherry-GFP-LC3 and plated to glass cover slips. After 24 h in culture, cells were fixed in 3% paraformaldehyde for 30 min, washed three times in PBS and then mounted onto glass slides. Cells were imaged on a Zeiss LSM 510-META Laser Scanning Confocal Microscope, as described above. Images were analyzed using NIH ImageJ software. They were first background subtracted and then thresholded using a tophat transform. The JACoP plugin (67) was used to perform object-based colocalization to determine the percent of puncta that are red-only (representing autolysosomes) or green-only (indicative of noise). To correct for noise, data were reported as %red-only−%green-only. To measure autolysosome life-time, cells were instead plated to chambered coverglasses and imaging was performed on a Deltavision-RT Live Cell Imaging System equipped with a Photometrics CoolSNAP HQ camera. A ×60 Olympus PlanApo N oil immersion objective with NA of 1.42 was used. Images were acquired in four z-stacks spaced at 0.75 μm to cover the full thickness of the cell, with a time interval of 20 s between stacks. Images were deconvolved, and z-stacks were then projected into a 2-D image. SoftWoRx 3.5.1 software was used for image acquisition, deconvolution and projection. Using NIH ImageJ software, image series were studied manually to identify events where yellow puncta became red, i.e. autophagosome-to-lysosome fusion events. From this point, frames were counted until the red punctum disappeared. This number was multiplied by 20 s to yield autolysosome lifetime. The apparent shape and intensity of vesicles were often influenced by their movement between z-planes or their simultaneous capture in multiple z-planes. These features were therefore not analyzed, and vesicles were regarded only as present or absent for the purpose of this analysis.

Cathepsin assay

Fibroblasts were plated to chambered coverglasses and imaged the following day on a Deltavision-RT Live Cell Imaging System. At the start of imaging, Magic Red reagent was diluted 1:365 into PBS, and then this solution was added at a 1:10 dilution into the cell culture media. Images were acquired using a ×20 Olympus UPlan objective, NA of 0.5, at 1 min intervals for a total of 20 min. Image analysis was performed using NIH ImageJ software. Images were thresholded to include only the lysosomal compartment, using the same numerical threshold for all images across a single experiment. The total fluorescence above threshold was normalized to the total area of the lysosomal compartment, measured as the area above threshold at $t = 20$ min. Normalized fluorescence intensities were plotted over time, and the slope of the line of best fit was determined by linear regression. To report relative cathepsin activity, the slope of each line was normalized within each experiment to the control group.

Lysosomal pH

Lysosomal pH was determined using ratiometric imaging of endocytosed Oregon Green Dextran (OGDx). Cells growing on chambered coverglasses were pulsed overnight with 150 μg/ml OGDx, and then chased for 4 h with the OGDx-free medium to ensure that all OGDx had arrived at its terminal location in the lysosome. Cells were then imaged on a Deltavision-RT Live Cell Imaging System as described above, with a ×40 UApo/340 oil immersion objective, NA of 1.35, using two filter pairs. The first (C1) used excitation/emission wavelengths of 436/535 nm; C2 was 492/535 nm. All imaging was performed at 37°C under 5% CO_2. A standard curve was constructed as described previously (27). Image analysis was performed using NIH ImageJ software. Each cell was analyzed independently. First, a binary image was generated by multiplying the two images (C1 × C2) and adjusting the intensity threshold to include only the labeled lysosomes. This image was then used as a mask for analysis of the original images. The integrated density of each image was measured and the ratio of integrated densities, C2/C1, was recorded. Using GraphPad Prism statistical software, the standards were fit to a sigmoidal curve by the least squares method, and unknowns were interpolated from this curve.

Statistics

For data with Gaussian distribution, statistical significance was assessed by unpaired Student's *t*-test (for comparison of two means) or ANOVA (for comparison of more than two means). The Newman–Keuls *post hoc* test was performed to carry out pairwise comparisons of group means if ANOVA rejected the null hypothesis. For non-Gaussian distributions (Fig. 2C), the Mann–Whitney test was used. Statistics were performed using the software package Prism 4 (GraphPad Software). *P*-values less than 0.05 were considered significant.

SUPPLEMENTARY MATERIAL

Supplementary Material is available at *HMG* online.

ACKNOWLEDGEMENTS

We thank James Shayman and Liming Shu for their advice and expertise in HPTLC lipid analysis, and for helping us to establish this method in our own laboratory. We thank Michael Davis with help measuring lysosomal pH.

Conflict of Interest statement: The authors have no conflict of interest to declare.

FUNDING

This work was supported by grants from the National Institutes of Health (grant number F31 NS065662 to M.J.E., R01 NS063967 to A.P.L.).

REFERENCES

1. Klionsky, D.J. (2005) The molecular machinery of autophagy: unanswered questions. *J. Cell Sci.*, **118**, 7–18.
2. Levine, B. and Kroemer, G. (2008) Autophagy in the pathogenesis of disease. *Cell*, **132**, 27–42.
3. Hara, T., Nakamura, K., Matsui, M., Yamamoto, A., Nakahara, Y., Suzuki-Migishima, R., Yokoyama, M., Mishima, K., Saito, I., Okano, H. *et al.* (2006) Suppression of basal autophagy in neural cells causes neurodegenerative disease in mice. *Nature*, **441**, 885–889.
4. Komatsu, M., Waguri, S., Chiba, T., Murata, S., Iwata, J., Tanida, I., Ueno, T., Koike, M., Uchiyama, Y., Kominami, E. *et al.* (2006) Loss of autophagy in the central nervous system causes neurodegeneration in mice. *Nature*, **441**, 880–884.
5. Ravikumar, B., Vacher, C., Berger, Z., Davies, J.E., Luo, S., Oroz, L.G., Scaravilli, F., Easton, D.F., Duden, R., O'Kane, C.J. *et al.* (2004) Inhibition of mTOR induces autophagy and reduces toxicity of polyglutamine expansions in fly and mouse models of Huntington disease. *Nat. Genet.*, **36**, 585–595.
6. Yue, Z., Horton, A., Bravin, M., DeJager, P.L., Selimi, F. and Heintz, N. (2002) A novel protein complex linking the delta 2 glutamate receptor and autophagy: implications for neurodegeneration in lurcher mice. *Neuron*, **35**, 921–933.
7. Nishiyama, J., Matsuda, K., Kakegawa, W., Yamada, N., Motohashi, J., Mizushima, N. and Yuzaki, M. (2010) Reevaluation of neurodegeneration in lurcher mice: constitutive ion fluxes cause cell death with, not by, autophagy. *J. Neurosci.*, **30**, 2177–2187.
8. Settembre, C., Fraldi, A., Jahreiss, L., Spampanato, C., Venturi, C., Medina, D., de Pablo, R., Tacchetti, C., Rubinsztein, D.C. and Ballabio, A. (2008) A block of autophagy in lysosomal storage disorders. *Hum. Mol. Genet.*, **17**, 119–129.
9. Banerjee, R., Beal, M.F. and Thomas, B. (2010) Autophagy in neurodegenerative disorders: pathogenic roles and therapeutic implications. *Trends Neurosci.*, **33**, 541–549.
10. Wilcox, W.R. (2004) Lysosomal storage disorders: the need for better pediatric recognition and comprehensive care. *J. Pediatr.*, **144**, S3–S14.
11. Vanier, M.T. and Millat, G. (2003) Niemann-Pick disease type C. *Clin. Genet.*, **64**, 269–281.
12. Carstea, E.D., Morris, J.A., Coleman, K.G., Loftus, S.K., Zhang, D., Cummings, C., Gu, J., Rosenfeld, M.A., Pavan, W.J., Krizman, D.B. *et al.* (1997) Niemann-Pick C1 disease gene: homology to mediators of cholesterol homeostasis. *Science*, **277**, 228–231.
13. Naureckiene, S., Sleat, D.E., Lackland, H., Fensom, A., Vanier, M.T., Wattiaux, R., Jadot, M. and Lobel, P. (2000) Identification of HE1 as the second gene of Niemann-Pick C disease. *Science*, **290**, 2298–2301.
14. Kwon, H.J., Abi-Mosleh, L., Wang, M.L., Deisenhofer, J., Goldstein, J.L., Brown, M.S. and Infante, R.E. (2009) Structure of N-terminal domain of NPC1 reveals distinct subdomains for binding and transfer of cholesterol. *Cell*, **137**, 1213–1224.
15. Pentchev, P.G., Comly, M.E., Kruth, H.S., Vanier, M.T., Wenger, D.A., Patel, S. and Brady, R.O. (1985) A defect in cholesterol esterification in Niemann-Pick disease (type C) patients. *Proc. Natl Acad. Sci. USA*, **82**, 8247–8251.
16. Karten, B., Peake, K.B. and Vance, J.E. (2009) Mechanisms and consequences of impaired lipid trafficking in Niemann-Pick type C1-deficient mammalian cells. *Biochim. Biophys. Acta*, **1791**, 659–670.
17. Ko, D.C., Milenkovic, L., Beier, S.M., Manuel, H., Buchanan, J. and Scott, M.P. (2005) Cell-autonomous death of cerebellar purkinje neurons with autophagy in Niemann-Pick type C disease. *PLoS Genet.*, **1**, 81–95.
18. Pacheco, C.D., Kunkel, R. and Lieberman, A.P. (2007) Autophagy in Niemann-Pick C disease is dependent upon Beclin-1 and responsive to lipid trafficking defects. *Hum. Mol. Genet.*, **16**, 1495–1503.
19. Klionsky, D.J., Abeliovich, H., Agostinis, P., Agrawal, D.K., Aliev, G., Askew, D.S., Baba, M., Baehrecke, E.H., Bahr, B.A., Ballabio, A. *et al.* (2008) Guidelines for the use and interpretation of assays for monitoring autophagy in higher eukaryotes. *Autophagy*, **4**, 151–175.
20. Higashi, Y., Murayama, S., Pentchev, P.G. and Suzuki, K. (1993) Cerebellar degeneration in the Niemann-Pick type C mouse. *Acta Neuropathol. (Berl.)*, **85**, 175–184.
21. Pacheco, C.D., Elrick, M.J. and Lieberman, A.P. (2009) Tau deletion exacerbates the phenotype of Niemann-Pick type C mice and implicates autophagy in pathogenesis. *Hum. Mol. Genet.*, **18**, 956–965.
22. Ordonez, M.P., Roberts, E.A., Kidwell, C.U., Yuan, S.H., Plaisted, W.C. and Goldstein, L.S. (2012) Disruption and therapeutic rescue of autophagy in a human neuronal model of Niemann Pick type C1. *Hum. Mol. Genet.*, **21**, 2651–2662.
23. Pankiv, S., Clausen, T.H., Lamark, T., Brech, A., Bruun, J.A., Outzen, H., Overvatn, A., Bjorkoy, G. and Johansen, T. (2007) p62/SQSTM1 binds directly to Atg8/LC3 to facilitate degradation of ubiquitinated protein aggregates by autophagy. *J. Biol. Chem.*, **282**, 24131–24145.
24. Turk, V., Turk, B. and Turk, D. (2001) Lysosomal cysteine proteases: facts and opportunities. *EMBO J.*, **20**, 4629–4633.
25. Holopainen, J.M., Saarikoski, J., Kinnunen, P.K. and Jarvela, I. (2001) Elevated lysosomal pH in neuronal ceroid lipofuscinoses (NCLs). *Eur. J. Biochem.*, **268**, 5851–5856.
26. Bach, G., Chen, C.S. and Pagano, R.E. (1999) Elevated lysosomal pH in Mucolipidosis type IV cells. *Clin. Chim. Acta*, **280**, 173–179.
27. Christensen, K.A., Myers, J.T. and Swanson, J.A. (2002) pH-dependent regulation of lysosomal calcium in macrophages. *J. Cell Sci.*, **115**, 599–607.
28. Liu, B., Turley, S.D., Burns, D.K., Miller, A.M., Repa, J.J. and Dietschy, J.M. (2009) Reversal of defective lysosomal transport in NPC disease ameliorates liver dysfunction and neurodegeneration in the npc1-/- mouse. *Proc. Natl Acad. Sci. USA*, **106**, 2377–2382.
29. Rosenbaum, A.I., Zhang, G., Warren, J.D. and Maxfield, F.R. (2010) Endocytosis of beta-cyclodextrins is responsible for cholesterol reduction in Niemann-Pick type C mutant cells. *Proc. Natl Acad. Sci. USA*, **107**, 5477–5482.
30. Singh, R., Kaushik, S., Wang, Y., Xiang, Y., Novak, I., Komatsu, M., Tanaka, K., Cuervo, A.M. and Czaja, M.J. (2009) Autophagy regulates lipid metabolism. *Nature*, **458**, 1131–1135.
31. Martin, S. and Parton, R.G. (2006) Lipid droplets: a unified view of a dynamic organelle. *Nat. Rev. Mol. Cell Biol.*, **7**, 373–378.
32. Rosenbaum, A.I., Rujoi, M., Huang, A.Y., Du, H., Grabowski, G.A. and Maxfield, F.R. (2009) Chemical screen to reduce sterol accumulation in Niemann-Pick C disease cells identifies novel lysosomal acid lipase inhibitors. *Biochim. Biophys. Acta*, **1791**, 1155–1165.
33. Kuma, A., Hatano, M., Matsui, M., Yamamoto, A., Nakaya, H., Yoshimori, T., Ohsumi, Y., Tokuhisa, T. and Mizushima, N. (2004) The role of autophagy during the early neonatal starvation period. *Nature*, **432**, 1032–1036.
34. Liscum, L. and Faust, J.R. (1989) The intracellular transport of low density lipoprotein-derived cholesterol is inhibited in Chinese hamster ovary cells cultured with 3-beta-[2-(diethylamino)ethoxy]androst-5-en-17-one. *J. Biol. Chem.*, **264**, 11796–11806.
35. German, D.C., Quintero, E.M., Liang, C., Xie, C. and Dietschy, J.M. (2001) Degeneration of neurons and glia in the Niemann-Pick C mouse is unrelated to the low-density lipoprotein receptor. *Neuroscience*, **105**, 999–1005.
36. Walkley, S.U. and Suzuki, K. (2004) Consequences of NPC1 and NPC2 loss of function in mammalian neurons. *Biochim. Biophys. Acta*, **1685**, 48–62.
37. Suzuki, K., Parker, C.C., Pentchev, P.G., Katz, D., Ghetti, B., D'Agostino, A.N. and Carstea, E.D. (1995) Neurofibrillary tangles in Niemann-Pick disease type C. *Acta Neuropathol.*, **89**, 227–238.

38. Davidson, C.D., Ali, N.F., Micsenyi, M.C., Stephney, G., Renault, S., Dobrenis, K., Ory, D.S., Vanier, M.T. and Walkley, S.U. (2009) Chronic cyclodextrin treatment of murine Niemann-Pick C disease ameliorates neuronal cholesterol and glycosphingolipid storage and disease progression. *PLoS ONE*, **4**, e6951.
39. Jahreiss, L., Menzies, F.M. and Rubinsztein, D.C. (2008) The itinerary of autophagosomes: from peripheral formation to kiss-and-run fusion with lysosomes. *Traffic*, **9**, 574–587.
40. Mortimore, G.E. and Poso, A.R. (1987) Intracellular protein catabolism and its control during nutrient deprivation and supply. *Annu. Rev. Nutr.*, **7**, 539–564.
41. Pfeifer, U. (1978) Inhibition by insulin of the formation of autophagic vacuoles in rat liver. A morphometric approach to the kinetics of intracellular degradation by autophagy. *J. Cell Biol.*, **78**, 152–167.
42. Amritraj, A., Peake, K., Kodam, A., Salio, C., Merighi, A., Vance, J.E. and Kar, S. (2009) Increased activity and altered subcellular distribution of lysosomal enzymes determine neuronal vulnerability in Niemann-Pick type C1-deficient mice. *Am. J. Pathol.*, **175**, 2540–2556.
43. Tamboli, I.Y., Hampel, H., Tien, N.T., Tolksdorf, K., Breiden, B., Mathews, P.M., Saftig, P., Sandhoff, K. and Walter, J. (2011) Sphingolipid storage affects autophagic metabolism of the amyloid precursor protein and promotes Abeta generation. *J. Neurosci.*, **31**, 1837–1849.
44. Zhang, M., Dwyer, N.K., Love, D.C., Cooney, A., Comly, M., Neufeld, E., Pentchev, P.G., Blanchette-Mackie, E.J. and Hanover, J.A. (2001) Cessation of rapid late endosomal tubulovesicular trafficking in Niemann-Pick type C1 disease. *Proc. Natl Acad. Sci. USA*, **98**, 4466–4471.
45. Lebrand, C., Corti, M., Goodson, H., Cosson, P., Cavalli, V., Mayran, N., Faure, J. and Gruenberg, J. (2002) Late endosome motility depends on lipids via the small GTPase Rab7. *EMBO J.*, **21**, 1289–1300.
46. Huynh, K.K., Gershenzon, E. and Grinstein, S. (2008) Cholesterol accumulation by macrophages impairs phagosome maturation. *J. Biol. Chem.*, **283**, 35745–35755.
47. Gutierrez, M.G., Munafo, D.B., Beron, W. and Colombo, M.I. (2004) Rab7 is required for the normal progression of the autophagic pathway in mammalian cells. *J. Cell Sci.*, **117**, 2687–2697.
48. Jager, S., Bucci, C., Tanida, I., Ueno, T., Kominami, E., Saftig, P. and Eskelinen, E.L. (2004) Role for Rab7 in maturation of late autophagic vacuoles. *J. Cell Sci.*, **117**, 4837–4848.
49. Pankiv, S., Alemu, E.A., Brech, A., Bruun, J.A., Lamark, T., Overvatn, A., Bjorkoy, G. and Johansen, T. (2010) FYCO1 is a Rab7 effector that binds to LC3 and PI3P to mediate microtubule plus end-directed vesicle transport. *J. Cell Biol.*, **188**, 253–269.
50. Mukherjee, S. and Maxfield, F.R. (2004) Lipid and cholesterol trafficking in NPC. *Biochim. Biophys. Acta*, **1685**, 28–37.
51. Korolchuk, V.I., Mansilla, A., Menzies, F.M. and Rubinsztein, D.C. (2009) Autophagy inhibition compromises degradation of ubiquitin-proteasome pathway substrates. *Mol. Cell*, **33**, 517–527.
52. Balch, W.E., Morimoto, R.I., Dillin, A. and Kelly, J.W. (2008) Adapting proteostasis for disease intervention. *Science*, **319**, 916–919.
53. Douglas, P.M. and Dillin, A. (2010) Protein homeostasis and aging in neurodegeneration. *J. Cell Biol.*, **190**, 719–729.
54. Auer, I.A., Schmidt, M.L., Lee, V.M., Curry, B., Suzuki, K., Shin, R.W., Pentchev, P.G., Carstea, E.D. and Trojanowski, J.Q. (1995) Paired helical filament tau (PHFtau) in Niemann-Pick type C disease is similar to PHFtau in Alzheimer's disease. *Acta Neuropathol. (Berl.)*, **90**, 547–551.
55. Bu, B., Li, J., Davies, P. and Vincent, I. (2002) Deregulation of cdk5, hyperphosphorylation, and cytoskeletal pathology in the Niemann-Pick type C murine model. *J. Neurosci.*, **22**, 6515–6525.
56. Spillantini, M.G., Tolnay, M., Love, S. and Goedert, M. (1999) Microtubule-associated protein tau, heparan sulphate and alpha-synuclein in several neurodegenerative diseases with dementia. *Acta Neuropathol. (Berl.)*, **97**, 585–594.
57. Saito, Y., Suzuki, K., Hulette, C.M. and Murayama, S. (2004) Aberrant phosphorylation of alpha-synuclein in human Niemann-Pick type C1 disease. *J. Neuropathol. Exp. Neurol.*, **63**, 323–328.
58. Saito, Y., Suzuki, K., Nanba, E., Yamamoto, T., Ohno, K. and Murayama, S. (2002) Niemann-Pick type C disease: accelerated neurofibrillary tangle formation and amyloid beta deposition associated with apolipoprotein E epsilon 4 homozygosity. *Ann. Neurol.*, **52**, 351–355.
59. Yu, W.H., Cuervo, A.M., Kumar, A., Peterhoff, C.M., Schmidt, S.D., Lee, J.H., Mohan, P.S., Mercken, M., Farmery, M.R., Tjernberg, L.O. *et al.* (2005) Macroautophagy—a novel Beta-amyloid peptide-generating pathway activated in Alzheimer's disease. *J. Cell Biol.*, **171**, 87–98.
60. Kubota, C., Torii, S., Hou, N., Saito, N., Yoshimoto, Y., Imai, H. and Takeuchi, T. (2010) Constitutive reactive oxygen species generation from autophagosome/lysosome in neuronal oxidative toxicity. *J. Biol. Chem.*, **285**, 667–674.
61. Elrick, M.J., Pacheco, C.D., Yu, T., Dadgar, N., Shakkottai, V.G., Ware, C., Paulson, H.L. and Lieberman, A.P. (2010) Conditional Niemann-Pick C mice demonstrate cell autonomous Purkinje cell neurodegeneration. *Hum. Mol. Genet.*, **19**, 837–847.
62. Shu, L., Lee, L. and Shayman, J.A. (2002) Regulation of phospholipase C-gamma activity by glycosphingolipids. *J. Biol. Chem.*, **277**, 18447–18453.
63. Shu, L., Murphy, H.S., Cooling, L. and Shayman, J.A. (2005) An *in vitro* model of Fabry disease. *J. Am. Soc. Nephrol.*, **16**, 2636–2645.
64. Ames, B.N. (1966) Assay of inorganic phosphate, total phosphate, and phosphatases. *Methods Enzymol.*, **8**, 115–118.
65. Abe, A., Arend, L.J., Lee, L., Lingwood, C., Brady, R.O. and Shayman, J.A. (2000) Glycosphingolipid depletion in fabry disease lymphoblasts with potent inhibitors of glucosylceramide synthase. *Kidney Int.*, **57**, 446–454.
66. Pipalia, N.H., Huang, A., Ralph, H., Rujoi, M. and Maxfield, F.R. (2006) Automated microscopy screening for compounds that partially revert cholesterol accumulation in Niemann-Pick C cells. *J. Lipid Res.*, **47**, 284–301.
67. Bolte, S. and Cordelieres, F.P. (2006) A guided tour into subcellular colocalization analysis in light microscopy. *J. Microsc.*, **224**, 213–232.